

# Galaxy Clusters in the Context of Superfluid Dark Matter

Alistair O. Hodson<sup>1</sup>, Hongsheng Zhao<sup>1</sup>, Justin Khoury<sup>2</sup>, and Benoit Famaey<sup>3</sup>

<sup>1</sup> School of Physics and Astronomy, University of St Andrews, Scotland

<sup>2</sup> Center for Particle Cosmology, Department of Physics and Astronomy, University of Pennsylvania, Philadelphia, PA 19104, USA

<sup>3</sup> Université de Strasbourg, CNRS UMR 7550, Observatoire astronomique de Strasbourg, 11 rue de l'Université, 67000 Strasbourg, France

e-mail: aoh2@st-andrews.ac.uk

November 21, 2016

## ABSTRACT

**Context.** Regarding the mass discrepancy issues in the Universe, the cold dark matter (CDM) paradigm and the Modified Newtonian Dynamics (MOND) paradigm are mutually exclusive in their issues and successes on large and small scales. It has recently been proposed, by assuming that dark matter is a superfluid, that MOND-like effects can be achieved on small scales whilst preserving the success of  $\Lambda$ CDM on large scales. Detailed models within this “superfluid dark matter” (SfDM) paradigm are yet to be constructed.

**Aims.** Here, we aim to provide the first set of spherical models of galaxy clusters in the context of SfDM. We aim to determine whether the superfluid formulation is indeed sufficient to explain the mass discrepancy in galaxy clusters.

**Methods.** The SfDM model is defined by two parameters,  $\Lambda$  which can be thought of as a mass scale in the Lagrangian of the scalar field effectively describing the phonons and which acts as a coupling constant between the phonons and baryons, and  $m$  the mass of the DM particles. Given these parameters, we outline the theoretical structure of the superfluid core and the surrounding “normal phase” dark halo of quasi-particles in thermal equilibrium. The latter should encompass the largest part of galaxy clusters. Here, we set the SfDM transition at the radius where the density and pressure of the superfluid and normal phase coincides, neglecting the effect of phonons in the superfluid core. We then apply the theory to a sample of galaxy clusters, and directly compare the SfDM predicted mass profiles to data.

**Results.** We find that the superfluid formulation can reproduce the X-ray dynamical mass profile of clusters, with less free parameters than the corresponding CDM fits with Navarro-Frenk-White (NFW) profiles. The SfDM fits however display slight under-predictions of the gravity in the central regions which might be partly related to our neglecting of the effect of phonons in these regions. The superfluid core radius is found to be of about  $36 (M_{\text{vir}}/(10^{15} M_{\odot}))^{1/6} (\Lambda m^3)^{-1/2}$  kpc where the SfDM parameter is  $\Lambda m^3 = 0.1 - 0.3 \times 10^{-3} \text{ eV}^4/c^8$  and  $M_{\text{vir}}$  is the virial mass.

**Conclusions.** We conclude that this superfluid formulation is successful in describing galaxy clusters, but further work will be needed to determine whether the parameter choice is consistent with galaxies. Our model could be made more realistic by exploring non-sphericity, the SfDM transition condition, and non-isothermal normal phase profiles.

**Key words.**

## 1. Introduction

While observations of large scale structure in the Universe are traditionally explained by invoking a non-uniform distribution of so-called dark matter (DM) particles, the nature of such particles and the strength of their interactions remain mysteries up to now. Such particles could actually be of any kind as long as they are collision-free non-relativistic massive particles on scales of galaxy clusters and above, as in the standard  $\Lambda$ CDM paradigm. A very common argument for the existence of such particles is the colliding bullet cluster (Clowe et al. 2006) which has a lensing signature offset from its baryonic centre. This is explained in the dark matter paradigm, as the gas of the cluster interacts while the dark matter does not and thus the gas stays closer to the center and the dark matter can pass through, almost unaffected. This therefore produces the observed lensing signature of the bullet cluster.

On smaller scales, however, there are issues with such interaction-free particle models, especially in explaining the dynamics of galaxies. The most discussed ones are the cusp-core, missing satellites, too big to fail, and satellite plane problems (e.g. Pawlowski et al. 2015). These issues have led a part of

the community to look away from the dark matter paradigm to explain the observed dynamics of galaxies. Indeed, the general problem of CDM in galaxies seems to be more profound than the series of problems listed above. In particular, one observes a diversity of shapes of rotation curves at a given maximal circular velocity scale, contrary to CDM expectations (Oman et al. 2015), and a uniformity of shapes at a given baryonic surface density scale (Famaey & McGaugh 2012). These puzzling observations can be summarized by the radial acceleration relation (McGaugh et al. 2016) which has been predicted more than 30 years ago by the Modified Newtonian Dynamics or MOND paradigm (Milgrom 1983a,b,c; Bekenstein & Milgrom 1984; Famaey & McGaugh 2012). This paradigm introduces an acceleration scale,  $a_0$ , directly enlightening the role actually played by the baryonic surface density in observations. When the gravitational acceleration is much larger than  $a_0$ , the gravity behaves as Newton predicts. Much below  $a_0$ , the force law of gravity switches to a force law proportional to  $1/r$  (rather than Newton's  $1/r^2$ ). MOND has had successes, not just in explaining rotation curves, but in explaining a large set of observations on galaxy scales (e.g. Famaey & McGaugh 2012). However, MOND has had little success with the large scales, e.g. galaxy clusters (see for example Sanders

1999) although work has been conducted to reconcile this problem with the inclusion of neutrinos (e.g. Sanders 2003; Angus et al. 2008; Angus 2009) or by modifying the MOND formulation itself (Zhao & Famaey 2012).

In short,  $\Lambda$ CDM seems to be successful on the large scales and weaker on the small scales and MOND seems to exhibit the exact opposite problem. It is therefore interesting to ask the question: can we have MOND behaviour on the small scales and dark matter-like behaviour on larger scales? Following up on previous proposals by, e.g., Blanchet & Heisenberg (2015), this is exactly what Khoury and Berezhiani recently explored in a series of papers (Khoury 2015; Berezhiani & Khoury 2015, 2016; Khoury 2016). The idea expressed in these works is the concept that there exists a dark matter contribution, but it behaves like a superfluid in cold enough and dense enough environments, typically within galaxies, and like particle dark matter (“normal phase”) in clusters and on larger scales. This framework aims to describe the rotation curve in galaxies via a MOND-like phonon-mediated force resulting from the dark matter when it is in its superfluid phase. Meanwhile, in galaxy clusters, most of the matter is outside the superfluid phase and is made of quasi-particles in thermal equilibrium.

Each paper discussed a different approach to achieve the desired effect, and we will focus here on Berezhiani & Khoury (2015) and Berezhiani & Khoury (2016). These two papers prescribe the fundamental components to the theory, but there are yet to be any attempts to make a detailed model of an astrophysical system. Further to the work in these two papers, we must also address how to model the normal phase of the matter and how that embeds the superfluid. In a first attempt to do this, we consider the case of spherical galaxy clusters. The reasons for choosing galaxy clusters rather than galaxies are 1) clusters are commonly modelled in spherical symmetry without the need for a disk component 2) in clusters there should be very little contribution from the phonon force and as a result, we can build a rather simplified model in this case.

Sec. 2 outlines how we model the dark matter, describing the superfluid phase, the normal phase, the modelling of how one phase transitions to the other and how we determine the virial mass and radius of the cluster in this context. In Sec. 3 we describe a toy model with no baryons for illustrative purposes. In Sec. 4 we analyze a sample of galaxy clusters in the context of superfluid, mainly comparing the derived mass profile of the superfluid to that calculated from hydrostatic equilibrium of the gas. We conclude in Sec. 5.

## 2. The Dark Matter Superfluid Model

In this section we will give a brief overview of the equations which describe a system in the context of the dark matter superfluid theory (SfDM). Let us first recall the general idea of the SfDM model. Ignoring interactions for simplicity, DM particles undergo a phase transition to the superfluid state whenever their de Broglie wavelength  $\lambda_{dB} \sim 1/mv$  is larger than the average interparticle separation  $\ell \sim n^{-1/3}$ . Here  $v$  is the DM velocity dispersion,  $m$  is the DM particle mass, and  $n$  is the local average DM number density. Thus superfluidity arises in sufficiently cold (large  $\lambda_{dB}$ ) and dense (small  $\ell$ ) environments. Another requirement for Bose-Einstein condensation is that DM reaches thermal equilibrium, which requires sufficiently strong self-interactions (Khoury 2015).

For the purpose of our analysis we will assume that thermal equilibrium is maintained throughout galaxy clusters. In this case we expect the superfluid phase to be confined within the

central regions of clusters, where the density is high enough. Because clusters are hotter than galaxies, most of their DM content will be in the normal phase. The DM in galaxy clusters therefore consists of a superfluid core, whose radius depending on parameter values will range from approximately 50 to 100 kpc, surrounded by an atmosphere of DM particles in the normal phase. The key element to model here will be the transition from one phase to the other. If too large a region in the cluster is in the superfluid phase, it is likely that observed X-ray gas temperature profiles will not be reproduced.

Within the superfluid core, DM is more aptly described as collective excitations, which at low energy are phonons. In the superfluid paradigm of Khoury (2015), the MOND-like effects are achieved as a result of phonon excitations in the superfluid phase mediating a long-range force between ordinary matter particles. This phonon-mediated force is only important at low acceleration ( $a \ll a_0$ ), resulting in strong deviations from Newtonian gravity. In galaxies, this effect is critical in reproducing the empirical success of MOND at fitting rotation curves. The central regions of galaxy clusters, however, tend to lie in the intermediate ( $a \sim a_0$ ) to Newtonian regime ( $a \gg a_0$ ), where the phonon-mediated force is at most comparable to the Newtonian force.<sup>1</sup> As a result, in galaxy clusters we expect that the phonon force will be unimportant compared to the DM component and therefore, in the interest of simplicity, we assume that the phonon contribution to our calculations is hereafter zero.<sup>2</sup>

### 2.1. Set Up

The gravitational potential  $\Phi$  is determined as usual by Poisson’s equation

$$\frac{1}{4\pi G_N} \nabla^2 \Phi(\mathbf{r}) = \rho + \rho_b(\mathbf{r}), \quad (1)$$

where  $\rho_b$  denotes the baryon mass density. This allows us to integrate for  $\Phi$  for any given equation of state  $\rho(\Phi)$ .

For simplicity we assume hydrostatic equilibrium, which requires

$$P = \int_r^\infty \rho \nabla \Phi \cdot d\mathbf{r}, \quad (2)$$

where  $\rho$  and  $P$  are the mass density and pressure of the DM, respectively. This allows us to obtain the pressure everywhere.

In the following we further assume spherical symmetry, in which case the above equations reduce to

$$\rho(r) + \rho_b = \frac{1}{4\pi G_N r} \frac{d^2(r\Phi)}{dr^2}; \quad (3)$$

and

$$\frac{dP}{dr} = -\rho \frac{d\Phi}{dr}. \quad (4)$$

To solve these equations and derive the DM profile in galaxy clusters, multiple parts of the model need to be addressed:

<sup>1</sup> We remind the reader that the MOND empirical law qualitatively consists of three regimes: the Newtonian regime ( $a \gg a_0$ ) where gravity is approximately Newtonian, the intermediate regime ( $a \sim a_0$ ) where deviations from Newtonian gravity are of order unity, and the deep-MOND regime ( $a \ll a_0$ ) where deviations from Newtonian are strong.

<sup>2</sup> Let us stress that this is in no way an acceptable assumption for galaxies. Thus some of the equations described in the following Sections cannot be applied to galaxies. One must include the phonon force for consistency.

- Dark matter superfluid core profile
- Dark matter normal halo profile
- Matching the superfluid core to the normal halo
- Determining the virial radius of the system
- Making total mass the free parameter

These ingredients will be described in turn below.

## 2.2. Dark Matter Superfluid Core

We begin by reviewing some properties of the the inner superfluid core, discussing the pressure, sound speed, gravitational potential, and how they are related.

Ignoring phonons, the pressure of the superfluid is related to its density  $\rho_s$  via (Berezhiani & Khoury 2015),

$$P_s = \frac{\rho_s^3}{12K^2}; \quad K \equiv \frac{\Lambda c^2 m^3}{\hbar^3}, \quad (5)$$

where  $\Lambda$  is a mass scale and  $c$  is the speed of light.<sup>3</sup> The superfluid parameters  $\Lambda$  and  $m$  always appear in the combination  $\Lambda m^3$  in our calculations, hence there exists a degeneracy when choosing values. We therefore combine the parameters in this way and will only discuss the value of  $K = \Lambda c^2 m^3 / \hbar^3$  in what follows.

Equation (5) describes a polytropic equation of state,  $P \sim \rho^{1+1/n}$ , with index  $n = 1/2$ . Substituting the superfluid equation of state in the equation of the hydrostatic equilibrium Eq. 4, we obtain

$$\frac{\rho_s}{4K^2} \frac{d\rho_s}{dr} = -\frac{d\Phi}{dr}. \quad (6)$$

It is easy to see that is solved by

$$\rho_s(r) = 2K \sqrt{-2\Phi(r)}. \quad (7)$$

Thus the superfluid density is uniquely specified once we know the gravitational potential. The latter is fixed by integrating Poisson's equation Eq. 3:

$$\frac{1}{4\pi G_N r^2} (r^2 \Phi'(r))' = 2K \sqrt{-2\Phi(r)} + \rho_b(r). \quad (8)$$

This can be solved with initial conditions,  $\Phi(r = 0) = \Phi_0$  and  $\Phi'(r = 0) = 0$  where  $\Phi_0$  is a free parameter to be determined.<sup>4</sup> We will discuss how we determine this central potential in Sec. 2.7.

Meanwhile, the adiabatic sound speed is as usual given by

$$c_s^2 = \frac{dP_s}{d\rho_s} = \left(\frac{\rho_s}{2K}\right)^2 = -2\Phi(r). \quad (9)$$

Thus the superfluid sound speed  $c_s$  is also simply related to the gravitational potential  $\Phi$ .

In the absence of baryons ( $\rho_b = 0$ ), Poisson's equation Eq. 8 can be cast as a Lane-Emden equation (Berezhiani & Khoury 2015). The resulting density profile is smooth at the origin, and vanishes at a certain radius, which defines the core radius. The latter is determined by the parameters of the model ( $m$  and  $\Lambda$ ) together with the central density. In the presence of baryons, the superfluid profile will of course be altered, but the characteristic feature of a superfluid profile vanishing at a particular radius will remain.

<sup>3</sup> We choose, in this work,  $\Lambda$  to be a mass scale to simplify the units of the  $\Lambda m^3$  combination which appears throughout. We will present  $\Lambda m^3$  in units of  $eV^4/c^8$ . However, we have made our equations dimensionally sound in real units such that  $\Lambda$  has units of mass,  $m$  has units of mass, and  $\hbar$  has normal units  $\text{kg m}^2 \text{s}^{-1}$ .

<sup>4</sup> The central potential gradient should really be set in accordance with the baryon potential gradient. However, setting our value to zero did not affect our results.

## 2.3. Dark Matter Normal Halo

The superfluid core is assumed to be surrounded by an atmosphere of normal-phase DM particles in thermal equilibrium. For simplicity we ignore interactions and treat this normal component as an ideal gas,

$$P_n = \frac{k_B T}{m} \rho_n. \quad (10)$$

Hydrostatic equilibrium in this case implies the well-known isothermal profile

$$\rho_n = \rho_0 \exp\left(-\frac{m\Phi(r)}{k_B T}\right). \quad (11)$$

In the simplified case where we omit the contribution of the baryons, substituting Eq. 11 into the Poisson Equation yields the simplified solution

$$\rho_n = \rho_c \left(\frac{R_c}{r}\right)^2. \quad (12)$$

The density normalization  $\rho_c$  and radius  $R_c$  will be fixed shortly.

Isothermal DM haloes have an enclosed mass which grows linearly with radius, resulting from the density  $\rho \propto r^{-2}$ . However, it is common in  $\Lambda$ CDM to model haloes using a Navarro-Frenk-White or NFW profile ((Navarro et al. 1997), (Zhao 1996)) which has, at large radius  $\rho \propto r^{-3}$  and a logarithmic mass growth. One should, for completeness, try several types of profile for the normal phase dark matter in the superfluid model. We will focus on the isothermal model in this work and explore other options in a future paper.

## 2.4. DM in two phases

Ideally one would like to build a model where there are three sections: 1) the inner section which is dominated by matter in the superfluid phase; 2) the outer halo which is dominated by normal phase matter; and 3) a transition regime where there is a mixture of normal phase and superfluid phase particles. We neglect this third regime in our model for simplicity and design a system where below the core radius,  $R_c$ , there exists only superfluid matter and above  $R_c$  there exists only normal phase matter. The procedure for determining this radius involves continuity of pressure between the two phases of dark matter and will be outlined in Sec. 2.5.

In other words, we model the DM in galaxy clusters as a superfluid core ( $r \leq R_c$ ) with density  $\rho_s = 2K \sqrt{-2\Phi(r)}$  and pressure  $P_s = \frac{\rho_s^3}{12K^2}$ , surrounded by a normal isothermal phase of DM in the outer halo ( $r \geq R_c$ ) with density  $\rho_n = \rho_c (R_c/r)^2$  and pressure  $P_n = \frac{k_B T}{m} \rho_n$ . The gravitational potential  $\Phi(r)$  has a meaningful zero point fixed by the central density of the superfluid, and  $K$  is a constant which is defined in Eq. 5. These two densities are meant to be continuous at the boundary, *i.e.*,  $\rho_s = \rho_n = \rho_c$  at  $r = R_c$ , although this boundary condition is independent of the coordinate system and spherical symmetry.<sup>5</sup>

<sup>5</sup> One could interpolate these two phases continuously using  $\rho = \rho_0(1 - m\Phi/k_B T/n)^n$ , where  $n \rightarrow 1/2$  we have the superfluid phase,  $n \rightarrow \infty$  we have the isothermal phase. Alternatively one could think of the real fluid being some superposition of the two fluid phases.

## 2.5. Matching the Superfluid Core to the Normal Halo

As mentioned above, we are assuming a model where the superfluid phase abruptly transitions into the normal phase of the fluid. We therefore have to determine at what radius this transition happens, which will define the core radius,  $R_c$ . The way we do this is by imposing the condition that the tangential pressure is continuous at the boundary between the core and normal phase dark matter. Therefore, the determined radius at which this criteria is satisfied is our core radius,  $R_c$ . We outline this procedure step by step.

### – Step 1: Calculating the Gravitational Enclosed Mass:

In order to perform the pressure matching routine, we must calculate the total enclosed gravitating mass (baryons + DM) as a function of radius, for  $r \geq R_c$ :

$$\begin{aligned} M_{\text{grav}}(r) &= M_c + M_n(r) + M_b(r) \\ &= 4\pi \int_0^{R_c} \rho_s(r') r'^2 dr' + 4\pi \int_{R_c}^r \rho_n(r') r'^2 dr' + M_b(r) \\ &= 8\pi \sqrt{2}K \int_0^{R_c} \sqrt{-\Phi(r)} r'^2 dr' + 4\pi R_c^2 \rho_c [r - R_c] \\ &\quad + M_b(r). \end{aligned} \quad (13)$$

The first term comes from integrating the superfluid density Eq. 7, the second from integrating the normal phase density Eq. 12, and the third is the baryonic mass. We therefore have the enclosed mass as a function of  $R_c$  and  $\rho_c$ .

### – Step 2: Solving the Poisson Equation:

Poisson's equation Eq. 8 is solved numerically given an initial value of the gravitational potential,  $\Phi_0$ , assuming the central gradient is zero. Doing this yields the gravitational potential profile  $\Phi(r)$ , which can be substituted to obtain the superfluid density profile  $\rho_s(r) = 2K \sqrt{-2\Phi(r)}$  as explained earlier. In our model, the superfluid density and gravitational potential profiles are only valid for  $r \leq R_c$ . The next step is to calculate  $R_c$ .

### – Step 3: Calculate the Core Radius:

As mentioned, we assume that the boundary between the normal and superfluid phase of the dark matter is the point at which the tangential pressures are equal. Mathematically, this means the point such that,

$$\frac{\rho_c^3}{12K^2} = \int_{R_c}^{\infty} \frac{\rho_n(r) G_N M_{\text{grav}}(r)}{r^2} dr = R_c^2 \rho_c \int_{R_c}^{\infty} \frac{G_N M_{\text{grav}}(r)}{r^4} dr. \quad (14)$$

The left hand side comes from the polytropic equation of state Eq. 5 describing the superfluid, with  $\rho_c = \rho_s(R_c)$ . The right hand side follows from hydrostatic equilibrium equation of the normal phase density, where we have substituted Eq. 12 for  $\rho_n(r)$ . Furthermore,  $M_{\text{grav}}(r)$  refers to the total enclosed mass (baryonic + dark mass) at radius  $r$ .

In order to solve Eq. 14 for the core radius  $R_c$ , we must write the parameters  $\rho_c$  and  $M_{\text{grav}}(r)$  as functions of  $R_c$ . The former is obtained by evaluating Eq. 7 at  $R_c$ :

$$\rho_c = \rho_s(R_c) = 2K \sqrt{-2\Phi(R_c)}. \quad (15)$$

For the enclosed mass  $M_{\text{grav}}(r)$ , note that the limits of the integral on the right hand side of Eq. 14 are greater than  $R_c$ ,

hence we can use our expression, Eq. (13), valid for  $r \geq R_c$ . Therefore by numerically solving Eq. 14 using derived expressions, for mass (Eq. 13) and core density (Eq. 15) we can determine a value for the core radius,  $R_c$ . From the calculated core radius, we can find the numerical value for the core density via Eq. 15.

## 2.6. Determining the Virial Radius

In the previous section we began by defining a central potential,  $\Phi_0$ , and from this we determined the core radius as well as the core density. We therefore have at our disposal all the necessary components to determine the density of the dark matter fluid both inside and outside the core.

The next stage is to determine the radius at which to truncate the DM halo. In the  $\Lambda$ CDM paradigm, this is commonly defined as  $r_{200}$ , the radius at which the average density falls to 200 times the critical density of the universe at a given redshift, *i.e.*, the virial density. We adopt this convention in our model. First, we should remind ourselves of the critical density, defined as

$$\rho_{\text{crit}}(z_{\text{vir}}) = \frac{3H^2(z_{\text{vir}})}{8\pi G_N}, \quad (16)$$

where  $H$  is the Hubble parameter determined from the background evolution, and  $z_{\text{vir}}$  is the redshift at which the cluster becomes virialized. The virial radius is then determined by solving

$$\frac{3M(R_{\text{vir}})}{4\pi R_{\text{vir}}^3} = 200\rho_{\text{crit}}(z_{\text{vir}}). \quad (17)$$

The mass  $M(R_{\text{vir}})$  is determined by evaluating Eq. 13.

## 2.7. Making Mass the Free Parameter

We have now determined everything needed to model a spherical system in the superfluid framework. However, this was achieved by initially solving Poisson's equation, which in turn required the input of the central potential  $\Phi_0$  as a free parameter. A more ideal set up would be to determine all relevant quantities,  $R_c$ ,  $\rho_c$ ,  $R_{\text{vir}}$  and  $\Phi_0$  from a known total mass  $M_{\text{vir}}$ . This is possible with the aid of interpolation. Basically, one can carry out the above procedure for a discrete set of  $n$  initial central potential values, say  $\{\Phi_{01}, \Phi_{02}, \dots, \Phi_{0n}\}$ . From this set one builds up an array of core radii,  $\{R_{c01}, R_{c02}, \dots, R_{c0n}\}$ , core densities  $\{\rho_{c01}, \rho_{c02}, \dots, \rho_{c0n}\}$ , virial radii  $\{R_{\text{vir}01}, R_{\text{vir}02}, \dots, R_{\text{vir}0n}\}$  and virial masses  $\{M_{\text{vir}01}, M_{\text{vir}02}, \dots, M_{\text{vir}0n}\}$ . One can then make list plots of  $\Phi_0$  vs  $M_{\text{vir}}$ ,  $R_c$  vs  $M_{\text{vir}}$ ,  $\rho_c$  vs  $M_{\text{vir}}$ , and  $R_{\text{vir}}$  vs  $M_{\text{vir}}$ . Then, interpolation procedures can be implemented to make continuous functions of virial mass as functions of core radius, core density, central potential and virial radius. This allows one to pick a virial mass and easily find the required parameters that describe the fluid.

## 3. A Worked Example Without Baryons

As a warm-up exercise, we illustrate our procedure for a DM-only galaxy cluster, *i.e.*, without baryons. Figure 1 shows the interpolation functions for the core radius  $R_c$ , density at core radius  $\rho_c$ , central potential  $\Phi_0$  and superfluid core mass  $M_c$  as functions of the virial mass  $M_{\text{vir}}$ , following the procedure outlined in Sec. 2.7. These allow us to determine the correct parameters for a given total virial mass. In this example we choose a total mass of  $10^{15} M_{\odot}$  at redshift  $z = 0$ .

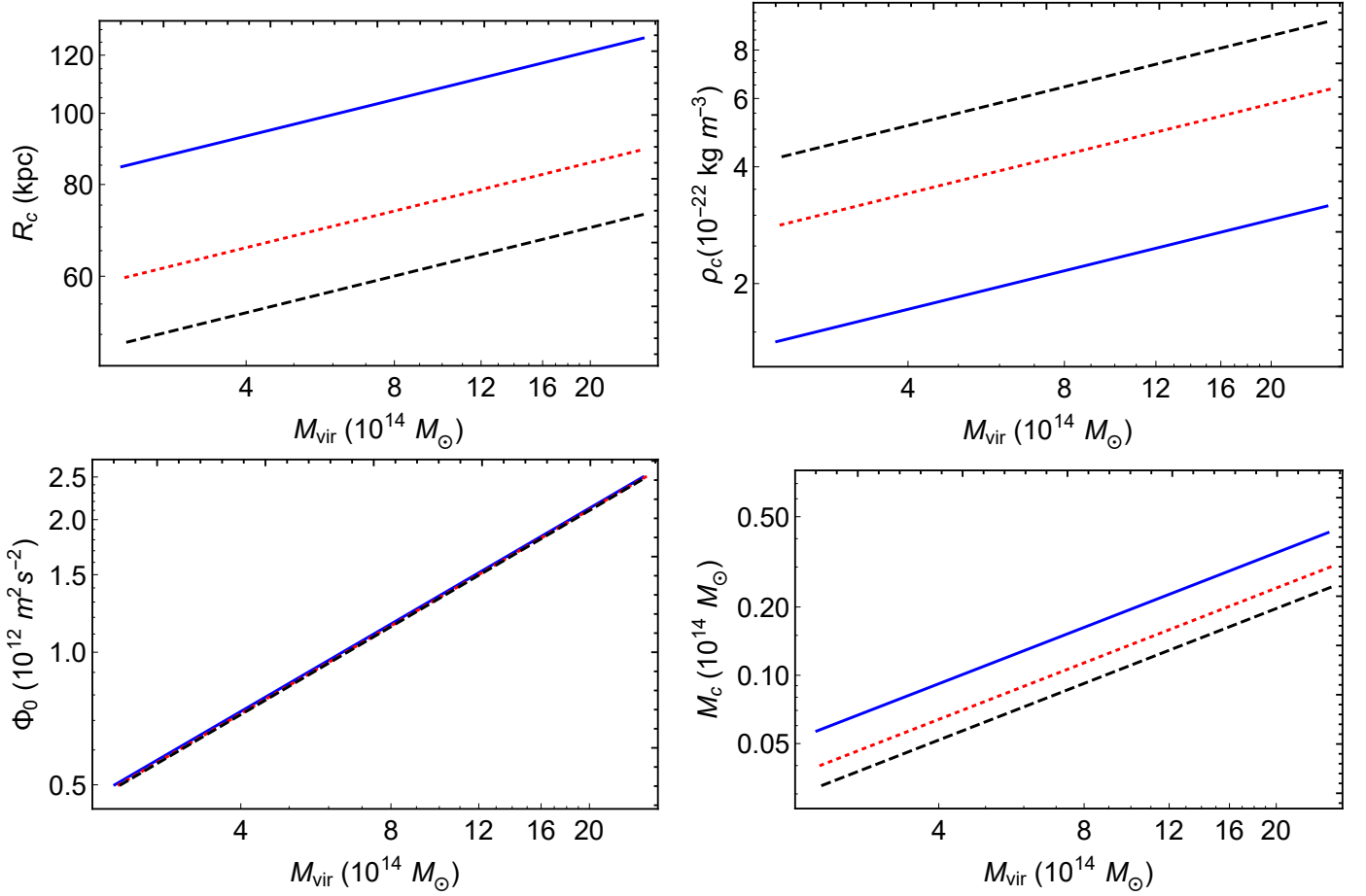


**Fig. 1.** Plots for our toy model of a dark matter only system. We highlight how parameters of the superfluid depend on the choice of virial mass for a system which only includes dark matter. One should stress the fact that this result does not consider baryons and a more complete analysis should be performed, which we provide for the cluster sample. If we were to include baryons, we would expect to see a slight decrease in core radius for our clusters. This difference would be enhanced in galaxies. Top Left: Plot showing the core radius vs virial mass. Top Right: Plot showing the density at the core radius vs virial mass. Bottom Left: Plot showing the central potential vs virial mass. Bottom Right: Plot showing the superfluid core mass vs virial mass. The three lines in each plot represent different choices of  $\Lambda m^3$ . Blue solid line has  $\Lambda m^3 = 0.1 \times 10^{-3} \text{ eV}^4/c^8$ , dotted red line has  $\Lambda m^3 = 0.2 \times 10^{-3} \text{ eV}^4/c^8$  and dashed black line has  $\Lambda m^3 = 0.3 \times 10^{-3} \text{ eV}^4/c^8$ .

Looking at Fig. 1, we see that  $R_c$ ,  $\rho_c$  and  $\Phi_0$  all scale with virial mass by power law profiles. We can try to understand this by analysing the model at the core radius. Firstly, ignoring baryons, Eq. 14 can be simplified to

$$\frac{\rho_c^2}{12K^2} = G_N \left( \frac{M_c}{R_c} - 2\pi R_c^2 \rho_c \right). \quad (18)$$

To understand the origin of the power laws, we will not perform a rigorous calculation, but rather use approximations and dimensional analysis to reason that the numerical results are reasonable. As mass is proportional to volume and density, we can make the approximate proportional relation,  $M_c \propto \rho_c R_c^3$ . Therefore Eq. 18 can be interpreted as  $\rho_c \propto R_c^2$ . We can also make the approximation that the velocity  $v$  is proportional to the virial velocity  $v_{\text{vir}}$ , which in turn we assume is proportional to the sound speed  $c_s$ . From our knowledge of the sound speed from Sec. 2.2 we know that  $c_s \propto \sqrt{\Phi}$ . From our Poisson equation we also know  $\sqrt{\Phi} \propto \rho_c$ . Therefore  $v_{\text{vir}} \propto \rho_c$ . The virial radius is related to the virial mass as  $R_{\text{vir}}^3 \propto M_{\text{vir}}$ . Thus from the relation for circular velocity, we get  $v_{\text{vir}} \propto M_{\text{vir}}^{1/3}$ . Collecting all these approx-

imations together, we get the following scaling relations,

$$\begin{aligned} \rho_c &\propto M_{\text{vir}}^{1/3} \\ R_c &\propto M_{\text{vir}}^{1/6} \\ \Phi_0 &\propto M_{\text{vir}}^{2/3} \\ M_c &\propto M_{\text{vir}}^{5/6}, \end{aligned} \quad (19)$$

which are in agreement with our numerical results. Although very informal, this analysis allows one to get an intuition as to how the quantities might scale with each other. These scaling relations however will not hold in the case when baryons are included.

We also show in Fig. 2 how varying the  $\Lambda m^3$  parameter affects the results. One can see that increasing  $\Lambda m^3$  results in a smaller  $R_c$ , larger  $\rho_c$  and smaller  $M_c$ , at the same virial mass. On the other hand,  $\Phi_0$  remains unchanged. Again this dependence can be understood on dimensional grounds. Specifically,

the  $\Lambda m^3$  scaling relations are

$$\begin{aligned} \rho_c &\propto \Lambda m^3 \\ R_c &\propto (\Lambda m^3)^{-1/2} \\ \Phi_0 &\propto (\Lambda m^3)^0 \\ M_c &\propto (\Lambda m^3)^{-1/2} \end{aligned} \quad (20)$$

These scaling relations can be understood by looking at the dimensionless form of Eqs. 8 and 14. Omitted here for conciseness, it can be shown that from the Poisson equation there arises a dimensionless core radius parameter,

$$x_c = \frac{\rho_c}{32\pi G K^2 R_c^2}. \quad (21)$$

This can also be understood from straightforward dimensional analysis; note that  $K$  has the dimension of density per velocity. The same  $x_c$  arises in the pressure balancing condition (Eq. 14), which then fixes  $x_c$  as a numerical constant for all halos. As  $x_c$  is constant, we gain information that  $\rho_c/R_c^2$  scale as  $K^2$ .

Under the condition of a small core, *i.e.*,  $R_c \ll R_{\text{vir}}$ , hence  $M_c \ll M_{\text{vir}}$ , we get, from Eq. 13, the relation

$$\frac{M_{\text{vir}}}{4\pi R_{\text{vir}}^3} = \rho_c R_c^2. \quad (22)$$

We therefore have two relations, which, together with  $R_{\text{vir}} \sim v_{\text{vir}} \sim M_{\text{vir}}^{1/3}$ , fix the scaling relations,  $\rho_c \sim K v_{\text{vir}}$ ,  $R_c \sim \sqrt{V_{\text{vir}}/K}/G$ . The potential  $\Phi_0 \sim G \rho_c R_c^2 \sim V_{\text{vir}}^2$  is independent of  $K$ . We can finally use Eq. 18 to find the  $M_c$  dependence.

These are in good agreement with the numerical results. To highlight this, in Figure 2 we plot the dependence of  $R_c$ ,  $\rho_c$  and  $M_c$  on  $\Lambda m^3$  for a fixed virial mass. We do not include the plot of  $\Phi_0$  as it is not affected by changing  $\Lambda m^3$ , which we did numerically check. One can see that Figure 2 follows the relationships shown in Eq. 20.

As we have the relationship of the superfluid parameters depend of the virial mass and  $\Lambda m^3$ , we can determine the correctly normalised scaling relations for the core radius, density at core radius, central potential and the core mass. These are,<sup>6</sup>

$$R_c \approx 36.2 \left( \frac{M_{\text{vir}}}{10^{15} M_\odot} \right)^{1/6} \left( \frac{\Lambda m^3}{10^{-3} \text{eV}^4/c^8} \right)^{-1/2} \text{ kpc}, \quad (23)$$

$$\rho_c \approx 2.1 \times 10^{-21} \left( \frac{M_{\text{vir}}}{10^{15} M_\odot} \right)^{1/3} \left( \frac{\Lambda m^3}{10^{-3} \text{eV}^4/c^8} \right) \text{ kg m}^{-3}, \quad (24)$$

$$M_c \approx 6.5 \times 10^{12} \left( \frac{M_{\text{vir}}}{10^{15} M_\odot} \right)^{5/6} \left( \frac{\Lambda m^3}{10^{-3} \text{eV}^4/c^8} \right)^{-1/2} M_\odot, \quad (25)$$

$$\Phi_0 \approx -1.3 \times 10^{12} \left( \frac{M_{\text{vir}}}{10^{15} M_\odot} \right)^{2/3} \text{ m}^2 \text{ s}^{-2}. \quad (26)$$

Of course these only rigorously apply for the situation where the baryon contribution is omitted.

<sup>6</sup> The scaling relations are approximate and will deviate slightly from the numerical solutions due to the approximations made. They are however useful as a rough estimate.

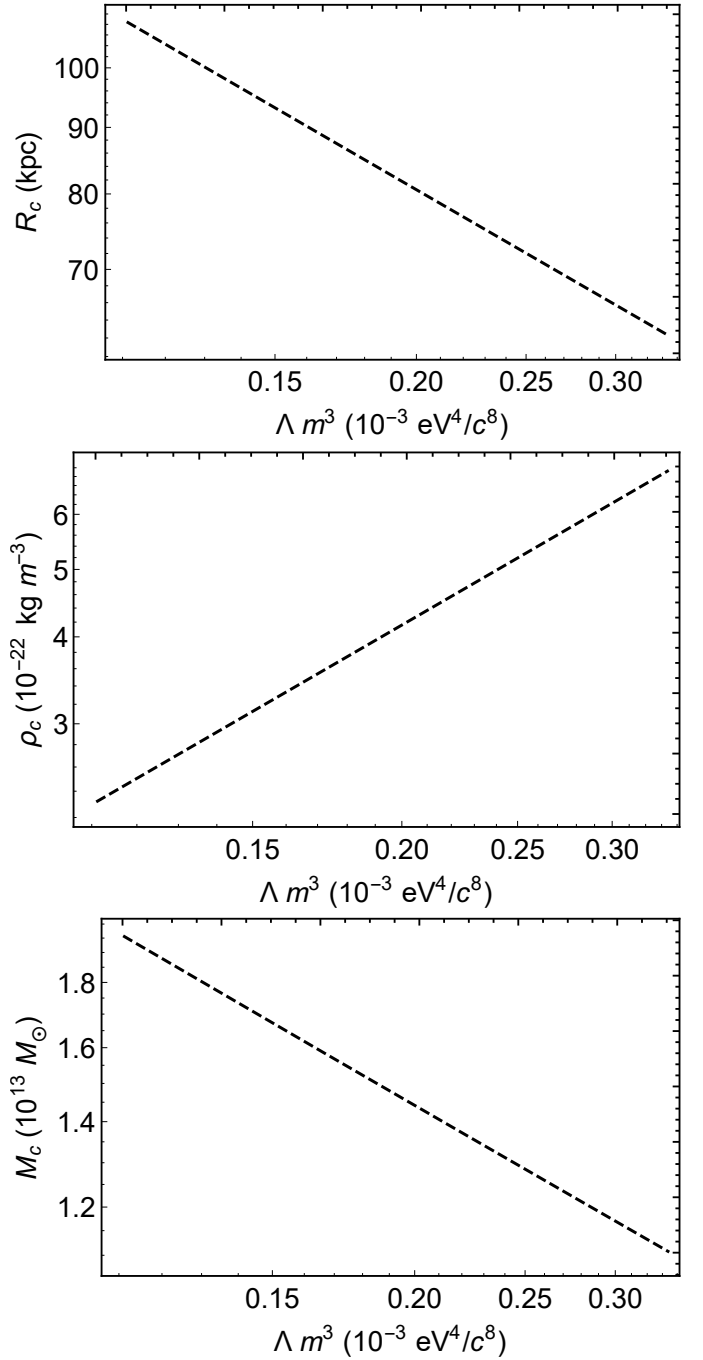


**Fig. 2.** Plot showing how the core radius (top panel), density at core radius (middle panel) and the core mass (bottom panel) change as a result of different values of  $\Lambda m^3$ . This is a visual representation of the relationships listed in Eq. 20.

Figure 3 shows the range of DM density profiles for our model for different parameter choices (blue shaded region), together with an NFW profile (black dashed line) for comparison. The virial mass is the same in the two cases,  $M_{\text{vir}} = 10^{15} M_\odot$ . The blue dots highlight the core radius for different choices of  $\Lambda m^3$ . We see that the superfluid density is relatively constant within the core, as expected. Outside the core the density profile smoothly transitions to the normal-phase, isothermal profile with  $\rho \sim 1/r^2$ . We can see from Fig. 3 that the core radius which we calculate is approximately 50-100 kpc for different parameter choices.

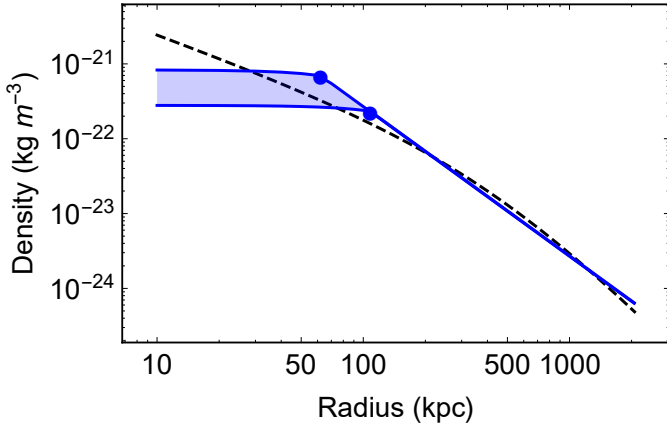


**Fig. 3.** Shows the DM only density profile for our SfDM toy model with  $\Lambda m^3 = 0.1 - 0.3 \times 10^{-3} \text{ eV}^4/c^8$  (blue shaded) and a  $c_{200} = 4$  NFW comparison profile (dashed black line) each with a virial mass of  $10^{15} M_\odot$ . Blue circles show the radii of the superfluid core for different  $\Lambda m^3$  choices (the upper line represents a larger choice of  $\Lambda m^3$ , which results in a higher density and smaller core radius). Inside the core, the density is approximately constant, outside the core the density follows a strict isothermal  $1/r^2$  power law. The inclusion of baryons in this model will not affect this over all features much, but will shrink the core radius slightly. The core radius can be increased by using a smaller value of  $\Lambda m^3$ , which we show in the following sections of the paper.

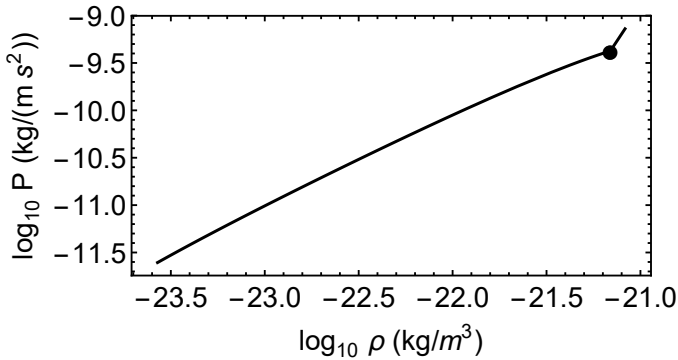


**Fig. 4.** Plot of pressure vs density for a dark matter only model. We can see from this that both the pressure and density are continuous, as per our phase transition requirements. At the core radius (black circle) there is a jump in gradient due to the discontinuity in the equation of state at the transition between the superfluid and normal phase of the dark matter. The core radius is located very close to the rightmost part of the plot as the density is approximately constant within the core.

We truncate the density to zero at the virial radius. If left untruncated, the enclosed mass would keep growing linearly, which is non-physical. Although the choice of the virial radius is somewhat arbitrary, as mentioned earlier we choose  $r_{200}$ , since this is commonly accepted in the  $\Lambda$ CDM literature.

To highlight the continuity of density and pressure, we show in Fig. 4 a pressure vs density plot. We can see from this that both the pressure and density are continuous and thus we have satisfied our phase matching criteria. However, one will notice that at the core radius, there is a sudden jump in gradient. This is due to our requirement that density and pressure must be continuous, but not a continuity of the equation of state. This results in a discontinuous sound speed, which we show in Figure 5. This is perhaps a limitation of our model and our simplified transition between the superfluid and normal phase of the dark matter. We do not address this matter here.

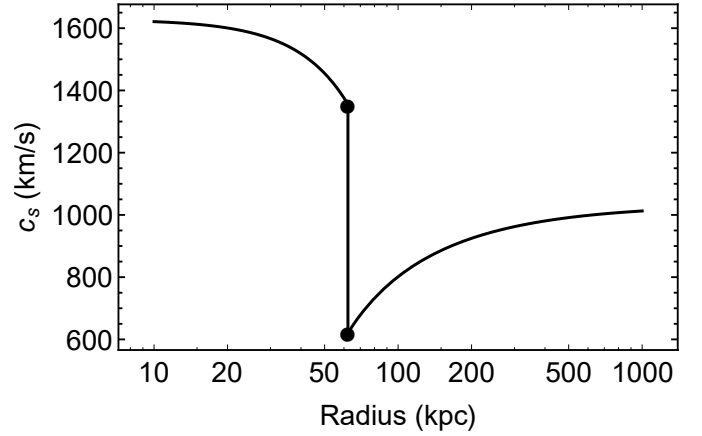


**Fig. 5.** Plot showing the sound speed of the dark matter ( $c_s^2 = dP/d\rho$ ). The jump at the core radius (vertical line) results from the discontinuous equation of state at the boundary. This might be a consequence of our simplified model of the phase transition. Addressing this issue is best left for future work.

We should also discuss one further consequence of our simplified model in reference to the core radius. We mentioned that in reality the superfluid core would continue radially until the density dropped to zero. Introducing this feature would make the model more complex as understanding how to define the normal phase profile becomes more challenging. This is the reason for adopting our two phase model with the core radius occurring when the density and tangential pressure are continuous. The result of this is a superfluid phase which has a much smaller radial extent than the true model and thus the core radii values we quote here are smaller than the true values. To highlight this, we plot the superfluid density profile for a dark matter only model, marking on the true core radius (black square), when  $\rho_s = 0$  and the core radius we adopt for this work (black circle) (Fig. 6). We can see that the true radius is approximately twice the value we determine from our pressure matching method. We can therefore conclude that we expect, in reality, superfluid phonon behaviour and dark matter contribution to occur at larger radii than we present here. This is an important point to note as the free parameter combination  $\Lambda m^3$  increases the superfluid dark matter density, at a cost of a smaller core radius in our model. If the core radius is too small, there could be contention with galaxy data as the phonon contribution (and hence MOND-like effects), which only exist within the superfluid phase, would not be sufficient. This could be an issue if we require a large  $\Lambda m^3$  value to fit clusters. We therefore stress that the core radius which we present here is the radius at which the pressure is matched and the superfluid effects will in reality extend much further.

For an actual galaxy cluster, to fit the data, one would take a similar approach to the  $\Lambda$ CDM paradigm and leave the virial mass of the cluster as a parameter to be fit. Unlike in the  $\Lambda$ CDM situation, the entire profile is determined from the mass alone whereas  $\Lambda$ CDM requires a second parameter, for example the concentration parameter  $c_{200}$ . There are other parameters to be determined in the superfluid model such as  $\Lambda$ ,  $m$  and also if one were to include the phonon force there are parameters  $\beta$  and  $\alpha$  (see Berezhiani & Khoury (2015), Berezhiani & Khoury (2016) for details on the scalar field phonon force), but these determine the property of the fluid and should be fixed for each cluster and galaxy. We have also assumed that the normal phase follows the isothermal profile where  $\rho \propto r^{-2}$ . As previously mentioned, one should investigate, for example, a  $\rho \propto r^{-3}$  profile which is more

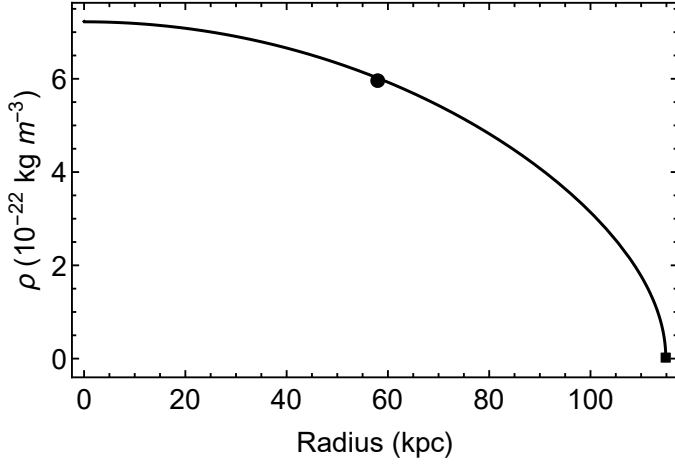


**Fig. 6.** Plot showing the density profile for a DM only system with central gravitational potential  $\Phi_0 = -10^{12} \text{ m}^2 \text{ s}^{-2}$ . The circle is the radius at which the tangential pressure is matched and the point where our model would transition to normal phase dark matter (what we call  $R_c$ ). The square is the radius at which the superfluid density drops to zero (the true extent of the superfluid matter). We show this to emphasise that our method truncates any superfluid effects at a much smaller radius than the true radius of the superfluid matter. This is a feature of our simplified model and more complex models will have to be constructed in future to fully understand the superfluid paradigm.

in line with the NFW profile commonly used to model particle dark matter.

#### 4. Application to Galaxy Cluster Mass Profiles

Now that the procedure for calculating the DM density profile has been outlined, we turn to a sample of galaxy clusters to see whether the superfluid provides a good description of the dynamics. In this paper we will focus on comparing the superfluid to the mass profile as derived from X-ray gas data. We intend to expand our analysis to cover weak gravitational lensing in a follow-up publication.

One method to determine how well the superfluid paradigm describes real galaxy clusters is to compare the expected dark matter profile, determined from the aforementioned model to the predicted mass of the galaxy clusters from the dynamics of the X-ray emitting gas. This amounts to a comparison of the enclosed mass derived from integrating the density profile, and the mass derived from hydrostatic equilibrium arguments. We have already discussed how one would calculate the enclosed mass derived from the density profile — see Eq. 13. We now briefly discuss how one derives the dynamical mass, *i.e.*, the mass derived from the X-ray gas emission profile.

Our treatment makes a number of simplifying assumptions which are common when modelling the mass profile of galaxy clusters. Firstly, the gas in the cluster is treated as an ideal gas,

$$P_g(r) = \frac{\rho_g(r) k_B T_g(r)}{w m_p}, \quad (27)$$

where  $\rho_g$  is the gas density,  $k_B T_g$  is the gas temperature,  $k_B$  is the Boltzmann constant, and  $m_p$  is the proton mass. Here,  $w$  is a parameter that describes the mean molecular weight of the gas, commonly taken to be  $w \approx 0.609$ . Secondly, the gas is assumed to be in hydrostatic equilibrium, such that

$$\frac{dP_g(r)}{dr} = -\rho_g(r) \frac{G_N M_{\text{dyn}}(r)}{r^2}, \quad (28)$$

where  $M_{\text{dyn}}(r)$  is the total dynamical (or total) mass of the system within radius  $r$ . We emphasise that the density is of the gas only.

Combining these two equations we obtain

$$-\frac{1}{\rho_g(r)} \frac{d}{dr} \left[ \frac{\rho_g(r) k_B T_g(r)}{w m_p} \right] = \frac{G_N M_{\text{dyn}}(r)}{r^2}. \quad (29)$$

The dynamical mass is defined as the required amount of mass such that the dynamics can be explained by Newtonian gravity. By applying some algebraic manipulation to Eq. 29, we arrive at the expression

$$M_{\text{dyn}}(r) = -\frac{k_B T(r) r}{G_N w m_p} \left[ \frac{d \ln \rho_g(r)}{d \ln r} + \frac{d \ln T(r)}{d \ln r} \right]. \quad (30)$$

This dynamical mass derived by fitting gas density and temperature of a cluster, can be compared to  $M_{\text{grav}}$  from Eq. 13 (which in  $\Lambda$ CDM and our superfluid cluster model would be baryons + dark matter)<sup>7</sup> to the dynamical mass. If these two masses are not equivalent, there is an issue with the gravitational paradigm in which we are working, assuming the object is in hydrostatic equilibrium and can be modelled accurately in spherical symmetry.

We have selected a sample of four galaxy clusters from Vikhlinin et al. (2006).<sup>8</sup> In this work, analytic profiles were prescribed for both the gas density and temperature. Fitting routines were then run to determine the parameters for each model. This allows the dynamical mass to be calculated analytically. Firstly, the gas emission profile is defined as,

$$n_e n_p(r) = n_0^2 \frac{(r/r_c)^{-\alpha}}{(1 + (r/r_c)^2)^{3\beta - \alpha/2}} \frac{1}{(1 + (r/r_s)^\gamma)^{\epsilon/\gamma}} + \frac{n_0^2}{(1 + (r/r_{c2})^2)^{3\beta_2}}. \quad (31)$$

such that the gas mass density is

$$\rho_g \approx 1.252 m_p \sqrt{n_e n_p}. \quad (32)$$

One can see from Eq. 31 that if parameters  $\alpha$  and  $\epsilon$  were set to zero, the emission profile would be equivalent to that of a superposition of two *beta* density profiles commonly used when describing galaxy gas density. Vikhlinin et al. (2006) added in the extra components to account for steepening brightness at  $r \approx 0.3 r_{200}$  and to impose a cuspy core to better match observations. More explicit details of this profile can be found in Vikhlinin et al. (2006).

The gas temperature profile is defined as,

$$T(r) = T_0 \frac{(r/r_{\text{cool}} + T_{\text{min}}/T_0)}{(r/r_{\text{cool}})^{a_{\text{cool}}} + 1} \frac{(r/r_t)^{-a}}{((r/r_t)^b + 1)^{c/b}}. \quad (33)$$

In Eq. 33, the term with subscript ‘cool’ models the observed cooling of X-ray gas in the inner radii of the cluster. The second term describes the temperature profile as a simple power law. Again more details on this temperature description can be found in Vikhlinin et al. (2006). The derived parameters can also be found in Vikhlinin et al. (2006).

<sup>7</sup> In MOND the gravitational mass would be baryons + phantom dark matter. There is a phantom component in the superfluid paradigm arising from the phonons, which should be negligible in clusters.

<sup>8</sup> At this stage we only test the model on a few clusters to gain an understanding of the current model predictions. We expect similar results for the other clusters in the Vikhlinin et al. (2006) sample and therefore see it sufficient to leave extending the sample size for future work when the model is developed further.



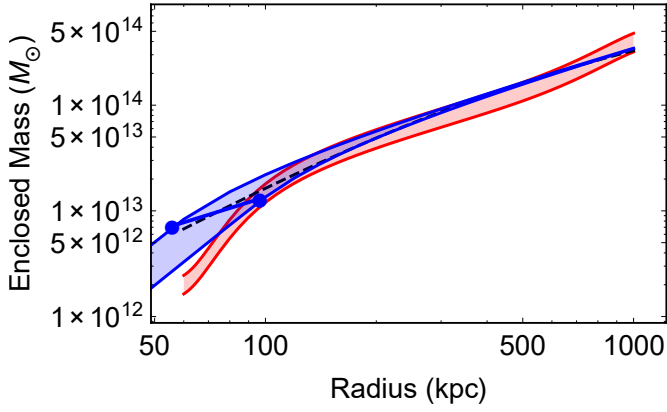


**Fig. 7.** Enclosed mass profiles for cluster A133. Red shaded regions are the  $\pm 20\%$  values of the dynamical mass calculated via Eq. 30. Blue shaded region is the mass profile of the SfDM paradigm to highlighting the  $\Lambda m^3$  dependence (upper and lower bands represent a larger and smaller choice of  $\Lambda m^3$  respectively). We choose parameters  $\Lambda m^3 = 0.1 - 0.3 \times 10^{-3} \text{ eV}^4/c^8$ . Black dashed line is the NFW profile as given in Vikhlinin et al. (2006). We have selected a virial mass of  $6 \times 10^{14} M_\odot$ . Blue circles show the positions superfluid core radii for the upper and lower choices of  $\Lambda m^3$ . We have tabulated the calculated SfDM parameters for the cluster in Table 1 and 2 for the different lower and upper bounds of  $\Lambda m^3$  respectively. We should also note that the best fit analytical gas and temperature profiles did not force monotonically increasing dynamical masses. To account for this, we removed non-physical features from the plot.

As well as the gas component, we should also take into account the brightest cluster galaxy (BCG) which is the large central galaxy component of the cluster. We model the baryonic component of the BCG using a Hernquist profile (Hernquist 1990),

$$\rho_{\text{BCG}}(r) = \frac{Mh}{2\pi r(r+h)^3}, \quad (34)$$

where  $M$  is the mass of the BCG and  $h$  is the BCG scale radius. The Hernquist profile is an appropriate choice for modelling the BCG baryonic mass content as it naturally provides a constant mass profile as large radii, resulting in a well defined size or radius of the BCG. Therefore no unnecessary truncation is required. We have adopted a BCG baryon mass of  $10^{12} M_\odot$  and a scale radius of 30 kpc. Though this is just an approximation. Therefore the baryonic mass which we use when deriving the dark matter profile is the sum of the BCG and the gas.

The derived mass profiles are plotted in Figs. 7, 8, 9 and 10. In these plots, we compare the superfluid mass (blue shaded region) to the dynamical mass (red shaded region). We also show the best-fit NFW dark matter profile as given in Vikhlinin et al. (2006) to compare the  $\Lambda$ CDM result to the superfluid result (black dashed line). For the latter, we do not numerically find the best fit parameters for the theory, but use the NFW predicted mass as a guide for what we think gives a reasonable fit to the data by eye. In practice, one should fit to find the best  $\Lambda$  and  $m$  parameters for the theory, but this should be done in accordance with galaxy rotation curves. This is not attempted in this work. We tabulate the derived superfluid parameters, mainly the core radius, density at the core radius and the central gravitational potential in Tables 1 and 2 for the upper and lower limit of  $\Lambda m^3$ . With these limitations, the superfluid gravitational mass seems to give a good representation to the dynamical mass in the outer radius of the clusters. For smaller radii, there seems to

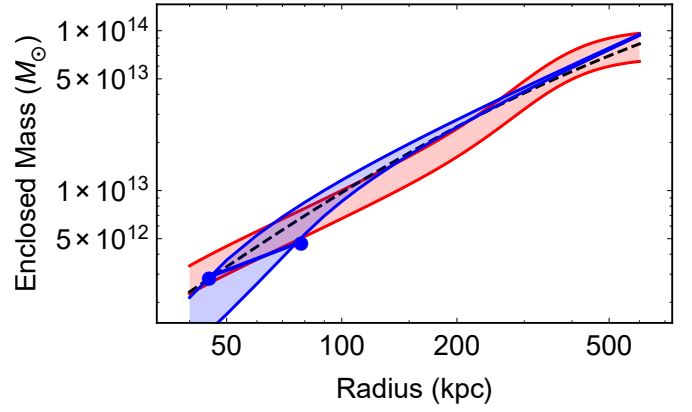


**Fig. 8.** Same as Fig. 7 for cluster A262. In this case we used a virial mass of  $2 \times 10^{14} M_\odot$ .

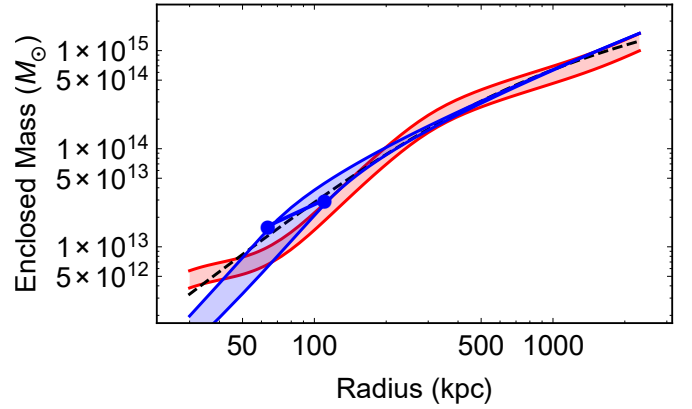


**Fig. 9.** Same as Fig. 7 for cluster A478. In this case we used a virial mass of  $1.5 \times 10^{15} M_\odot$ .

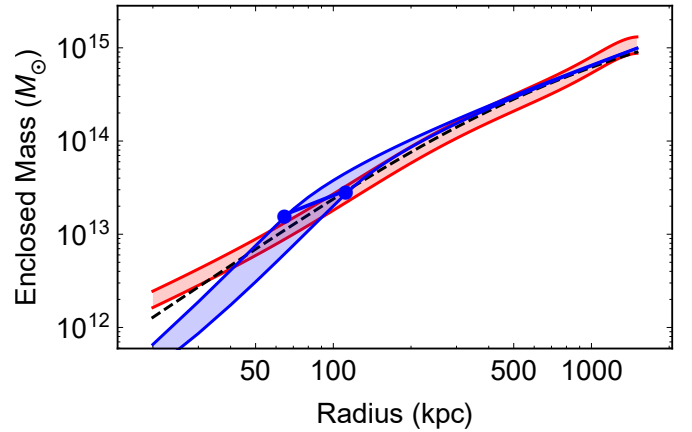


**Fig. 10.** Same as Fig. 7 for cluster A1413. In this case we used a virial mass of  $1.5 \times 10^{15} M_\odot$ .

a mismatch as the superfluid gravitational mass seems to generally under-predict the dynamical mass in our small sample. This under-prediction is mainly due to the constant density core which the theory predicts. We can achieve a better match in the centre by increasing the value of  $\Lambda m^3$  at a price of a smaller superfluid core.

We see from Figures 7- 10 how the choice of  $\Lambda m^3$  affects the mass profile. In these plots, an increasing mass corresponds to an increasing value for  $\Lambda m^3$ , we choose values ranging from  $\Lambda m^3 = 0.1 - 0.3 \times 10^{-3} \text{ eV}^4/c^8$ . If, for example, the mass of the

**Table 1.** Table showing the parameters which define clusters A133, A262, A478 and A1413 for  $\Lambda m^3 = 0.1 \times 10^{-3} \text{ eV}^4/c^8$ . Columns in order are 1) Cluster name, 2) virial mass used for cluster, 3) superfluid core radius, 4) central gravitational potential, 5) dark matter density at core radius. The virial radius is independent of the superfluid framework, assuming we can apply  $\Lambda$ CDM cosmology, and thus is not shown here.

Cluster	$M_T (M_\odot)$	$R_c (\text{kpc})$	$\Phi_0 (\text{m}^2\text{s}^{-2})$	$\rho_c (\text{kg m}^{-3})$
A133	$6.0 \times 10^{14}$	96.89	$-9.74 \times 10^{11}$	$1.96 \times 10^{-22}$
A262	$2.0 \times 10^{14}$	78.43	$-5.60 \times 10^{11}$	$1.35 \times 10^{-22}$
A478	$1.5 \times 10^{15}$	110.65	$-1.95 \times 10^{12}$	$2.69 \times 10^{-22}$
A1413	$1.5 \times 10^{15}$	112.36	$-1.93 \times 10^{12}$	$2.69 \times 10^{-22}$

**Table 2.** Same as table 1 for for  $\Lambda m^3 = 0.3 \times 10^{-3} \text{ eV}^4/c^8$ .

Cluster	$M_T (M_\odot)$	$R_c (\text{kpc})$	$\Phi_0 (\text{m}^2\text{s}^{-2})$	$\rho_c (\text{kg m}^{-3})$
A133	$6.0 \times 10^{14}$	55.91	$-9.37 \times 10^{11}$	$5.77 \times 10^{-22}$
A262	$2.0 \times 10^{14}$	45.09	$-5.31 \times 10^{11}$	$3.70 \times 10^{-22}$
A478	$1.5 \times 10^{15}$	64.08	$-1.84 \times 10^{12}$	$7.09 \times 10^{-22}$
A1413	$1.5 \times 10^{15}$	64.96	$-1.84 \times 10^{12}$	$7.95 \times 10^{-22}$

**Table 3.** Table showing how the core radius, core density and central potential change with choice of  $\Lambda m^3$  for cluster A133. Columns in order from left to right are 1) value of  $\Lambda m^3$ , 2) value of the core radius, 3) value of density at the core radius, 4) value of the gravitational potential at  $r \approx 0$  (not exactly  $r = 0$  for numerical reasons). The value of  $\Phi_0$  has small changes due to the introduction of baryons where our DM-only analysis showed that there should be no change in  $\Phi_0$  when we change  $\Lambda m^3$ .

$\Lambda m^3 (10^{-3} \text{ eV}^4/c^8)$	$R_c (\text{kpc})$	$\rho_c (\text{kg m}^{-3})$	$\Phi_0 (\text{m}^2\text{s}^{-2})$
0.1	96.89	$1.96 \times 10^{-22}$	$-9.74 \times 10^{11}$
0.15	79.08	$2.91 \times 10^{-22}$	$-9.59 \times 10^{11}$
0.2	68.48	$3.87 \times 10^{-22}$	$-9.49 \times 10^{11}$
0.25	61.25	$4.82 \times 10^{-22}$	$-9.42 \times 10^{11}$
0.3	55.91	$5.77 \times 10^{-22}$	$-9.37 \times 10^{11}$

dark matter particle was fixed at 0.6 eV, this would correspond to  $\Lambda \approx 0.4 - 1 \times 10^{-3} \text{ eV}/c^2$ . For one cluster, A133, we also tabulate the values for the core radius, core density, virial radius and central potential for each choice of  $\Lambda m^3$  (Table 3).

What we find is that for an increasing value of  $\Lambda m^3$  we find the core radius significantly decreases. It then follows that as the clusters tend to prefer a larger value of the  $\Lambda m^3$ , the clusters prefer to have a small core radius with the majority of the cluster being dominated by the normal phase dark matter. Future work with galaxies and rotation curves should provide further constraints on this parameter choice.

We also compare the derived interpolation functions for the core radius, core density, central potential and virial radius for two values for the BCG mass to determine how the baryonic mass affects the parameter values (Fig. 11). Clearly, the virial radius is unchanged for each choice of mass as it is solely determined by the virial density, which is cosmologically determined. The core radius decreases with a larger mass BCG, but the central core and central potential both increase. Having said this, for the high mass end of the functions, there is relatively small dif-

ference in the parameters and thus we can safely say that the altering the toy BCG model we add to the cluster gas mass should not affect the results significantly.

## 5. Discussion and Conclusion

In this paper, we have outlined a procedure for calculating spherical cluster models, embedded in a dark matter halo consisting of a superfluid. The model assumes that the dark matter exists in two distinct phases, a superfluid core and a normal phase halo. We do not take into consideration the possibility that there exists a transition region, where there is a mixture of superfluid and normal phase dark matter. This is left for further work. We also make the assumption that the normal component follows a isothermal profile which has  $\rho \propto r^{-2}$ . Further work should consider a  $\rho \propto r^{-3}$  or even a mixture of both. We have also assumed that the phonon contribution to the force is negligible. We believe this to be a valid approximation as the phonon contribution adds a MOND-like force, which is known to be comparatively weak in clusters. This is certainly not valid in galaxies.

We apply our model to a set of galaxy clusters, comparing the mass derived from hydrostatic equilibrium and that of our superfluid. We have not attempted to to a rigorous error analysis and  $\chi$  squared fitting of the superfluid mass and the parameters which describe the superfluid. This should be done in conjunction with galaxies. Modelling galaxies is a much more complicated procedure as one must understand how to model the phonon contribution and perhaps think about relaxing the spherical symmetry assumptions in order to correctly model disks. It is for these reasons that galaxies should be left for further analysis. That being said, one would hope that the superfluid parameters which are used in the cluster calculation are consistent with galaxies. Therefore this work should give a guide for fitting galaxies. One point which should be noted is that a larger value of  $\Lambda m^3$  seemed to be preferred by the clusters. This in turn decreases the core radius of the superfluid. One must ensure this does not cause issues with fitting galaxies as galaxies should be mainly inside the superfluid core.

There is a little tension between the superfluid result and the dynamical mass estimates of the cluster. For smaller values of  $\Lambda m^3$ , the superfluid core seems to systematically under-predict the galaxy cluster mass (except in cluster A133). This seems to be a result of the superfluid recipe predicting a constant density core where as the data seems to prefer a cuspiest core. This should be rigorously tested against strong lensing data of galaxy clusters as an independent test. We do achieve better fits with a larger choice of  $\Lambda m^3$  at the cost of a smaller core radius. which could be in contention with galaxy data. However, as we mentioned, the true extent of the superfluid core will be larger than our quoted values, so this may not be an issue.

We have in this work presented a simplified model of superfluid and perhaps the inclusion of the phonon force and a mixed phase consisting of both normal and superfluid dark matter may produce a cuspiest core. In short, our assumptions of the inner regions may be the root cause of the discrepancy with data. Also, once the phonon contribution is included, the best-fit parameters for  $\Lambda m^3$  could actually become smaller to accomodate for a core shrinking too much in the presence of phonons compared to the present calculations.

The next goal would be to perform lensing tests with galaxy clusters in the superfluid paradigm as an independent test. Once this is completed, one should move on to model galaxies, with an understanding of how the phonon force should be handled.

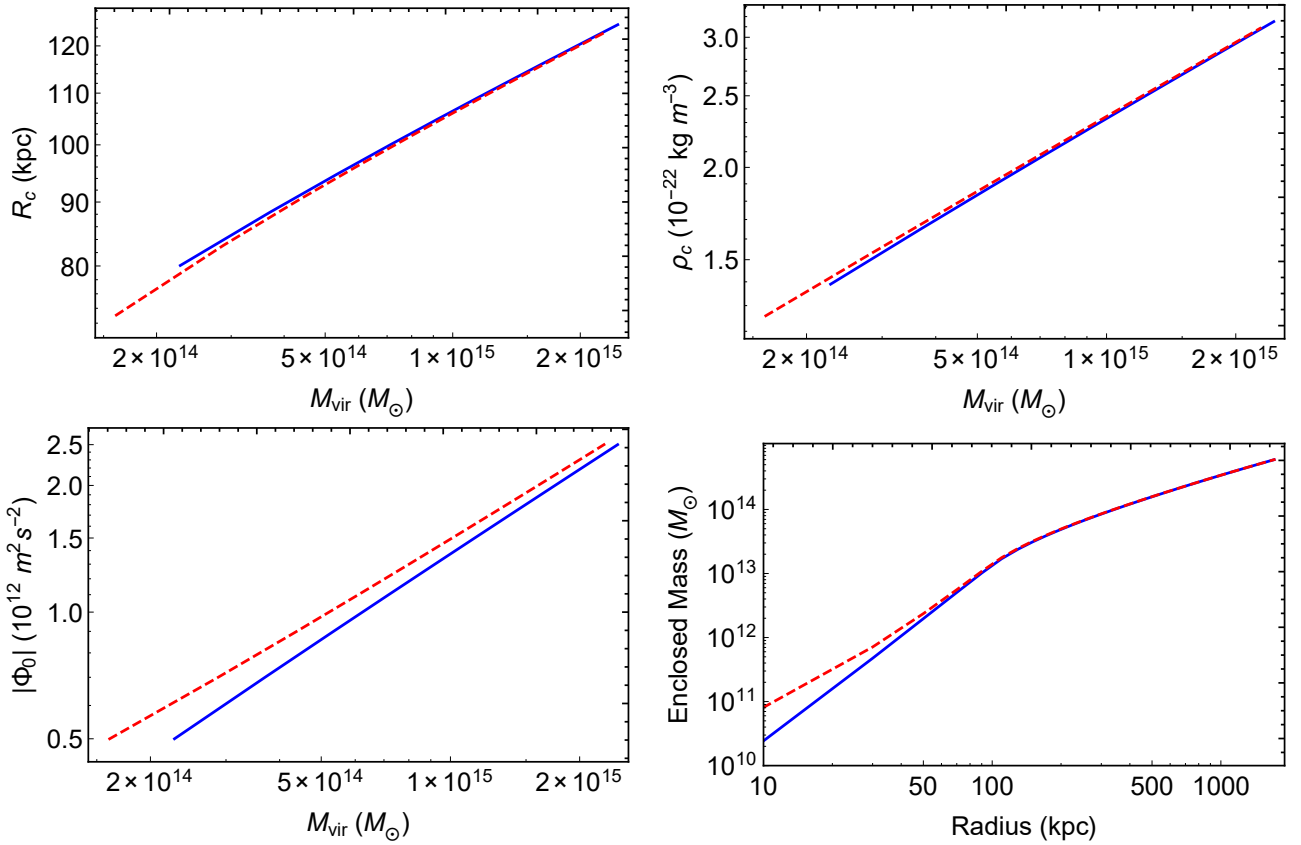


**Fig. 11.** Plots for cluster A133 for two choices of BCG mass,  $10^{11} M_{\odot}$  (Red dashed lines) and  $10^{12} M_{\odot}$  (Blue solid lines). Top left: Plot showing the core radius vs virial mass. Top right: Plot showing the density at the core radius vs virial mass. Bottom left: Plot showing the central potential vs virial mass. Bottom right: Plot showing the enclosed mass profile as a function of radius. We use a virial mass of  $6 \times 10^{14} M_{\odot}$  and a value of  $\Lambda m^3 = 0.1 \times 10^{-3} \text{ eV}^4/c^8$  for each plot.

In order to do this, one may need to construct a more complicated model, with the inclusion of a transition region between the superfluid and normal phase.

## Acknowledgements

We thank Lasha Berezhiani for helpful discussions. We also thank Alexey Vikhlinin for helpful correspondence on the cluster data. We warmly thank Priya Natarajan and Doug Finkbeiner for hosting a stimulating Radcliffe Exploratory Seminar at Harvard University where this collaboration was initiated. AOH is supported by Science and Technologies Funding Council (STFC) studentship (Grant code: 1-APAA-STFC12). J.K. is supported in part by NSF CAREER Award PHY-1145525, NASA ATP grant NNX11AI95G, and the Charles E. Kaufman Foundation of the Pittsburgh Foundation. BF acknowledges the financial support from the “Programme Investissements d’Avenir” (PIA) of the IdEx from the Université de Strasbourg.

## References

- Angus, G. W. 2009, MNRAS, 394, 527  
 Angus, G. W., Famaey, B., & Buote, D. A. 2008, MNRAS, 387, 1470  
 Bekenstein, J. & Milgrom, M. 1984, ApJ, 286, 7  
 Berezhiani, L. & Khoury, J. 2015, Phys. Rev. D, 92, 103510  
 Berezhiani, L. & Khoury, J. 2016, Physics Letters B, 753, 639  
 Blanchet, L. & Heisenberg, L. 2015, Phys. Rev. D, 91, 103518  
 Clowe, D., Bradač, M., Gonzalez, A. H., et al. 2006, ApJ, 648, L109  
 Famaey, B. & McGaugh, S. S. 2012, Living Reviews in Relativity, 15 [arXiv:1112.3960]  
 Hernquist, L. 1990, ApJ, 356, 359

- Khoury, J. 2015, Phys. Rev. D, 91, 024022  
 Khoury, J. 2016, Phys. Rev. D, 93, 103533  
 McGaugh, S., Lelli, F., & Schombert, J. 2016, Phys. Rev. Lett. [arXiv:1609.05917]  
 Milgrom, M. 1983a, ApJ, 270, 371  
 Milgrom, M. 1983b, ApJ, 270, 384  
 Milgrom, M. 1983c, ApJ, 270, 365  
 Navarro, J. F., Frenk, C. S., & White, S. D. M. 1997, ApJ, 490, 493  
 Oman, K. A., Navarro, J. F., Fattahi, A., et al. 2015, MNRAS, 452, 3650  
 Pawlowski, M. S., Famaey, B., Merritt, D., & Kroupa, P. 2015, ApJ, 815, 19  
 Sanders, R. H. 1999, ApJ, 512, L23  
 Sanders, R. H. 2003, MNRAS, 342, 901  
 Vikhlinin, A., Kravtsov, A., Forman, W., et al. 2006, ApJ, 640, 691  
 Zhao, H. 1996, MNRAS, 278, 488  
 Zhao, H. & Famaey, B. 2012, Phys. Rev. D, 86, 067301